Inorg. Chem. **2005**, *44*, 2407–2413

Analysis of the Spin Exchange Interactions and the Ordered Magnetic Structures of Lithium Transition Metal Phosphates $LiMPO_4$ (M = Mn, Fe, Co, Ni) with the Olivine Structure

D. Dai and M.-H. Whangbo*

Department of Chemistry, North Carolina State University, Raleigh, North Carolina 27695-8204

H.-J. Koo*

Department of Chemistry and Institute of Basic Science, Kyung Hee University, Seoul 130-701, South Korea

X. Rocquefelte and S. Jobic*

Institut des Matériaux Jean Rouxel, UMR 6502 Université de Nantes-CNRS, Laboratoire de Chimie des Solides, 2 rue de la Houssinière, BP 32229, 44322 Nantes Cedex 3, France

A. Villesuzanne*

ICMCB-CNRS, 87, avenue du Dr. A. Schweitzer, 33608 Pessac Cedex, France

Received November 8, 2004

The olivine-type compounds $LiMPO_4$ (M = Mn, Fe, Co, Ni) consist of MO_4 layers made up of corner-sharing MO_6 octahedra of high-spin M^{2+} ions. To gain insight into the magnetic properties of these phosphates, their spin exchange interactions were estimated by spin dimer analysis using tight binding calculations and by electronic band structure analysis using first principles density functional theory calculations. Three spin exchange interactions were found to be important for $LiMPO_4$, namely, the intralayer superexchange J_1, the intralayer super-superexchange J_b along the *b*-direction, and the interlayer super-superexchange J_2 along the *b*-direction. The magnetic ground state of $LiMPO_4$ was determined in terms of these spin exchange interactions by calculating the total spin exchange interaction energy under the classical spin approximation. In the spin lattice of $LiMPO_4$, the two-dimensional antiferromagnetic planes defined by the spin exchange J_1 are antiferromagnetically coupled by the spin exchange J_2, in agreement with available experimental data.

1. Introduction

Recently lithium transition metal phosphates $LiMPO_4$ (M = Mn, Fe, Co, Ni) with the olivine structure have received much attention as high-potential cathode materials for rechargeable Li-ion batteries.[1−9] The origin of the high electrochemical potentials these materials generate has been examined in several first principles electronic structure studies.[9−11] These phosphates contain high-spin M^{2+} ions.

* Authors to whom correspondence should be addressed. E-mail: mike_whangbo@ncsu.edu (M.-H.W.); hjkoo@khu.ac.kr (H.-J.K.); stephane.jobic@cnrs-imn.fr (S.J.); ville@icmcb-bordeaux.cnrs.fr (A.V.).

(1) Padhi, A. K.; Nanjundaswamy, K. S.; Goodenough, J. *J. Electrochem. Soc.* **1997**, *144*, 1188.
(2) Padhi, A. K.; Nanjundaswamy, K. S.; Masquelier, C.; Okada, S.; Goodenough, J. *J. Electrochem. Soc.* **1997**, *144*, 1609.
(3) Yamada, A.; Chung, S.-C.; Hinokuma, K. *J. Electrochem. Soc.* **2001**, *148*, A224.
(4) Huang, H.; Yin, S.-C.; Nazar, L. F. *Electrochem. Solid-State Lett.* **2001**, *4*, A170.
(5) Franger, S.; Le Cras, F.; Bourbon, C.; Rouault, H. *Electrochem. Solid-State Lett.* **2002**, *5*, A231.
(6) Yamada, A.; Chung, S.-C. *J. Electrochem. Soc.* **2001**, *148*, A960.
(7) Li, G.; Azuma, H.; Tohda, M. *Electrochem. Solid-State Lett.* **2002**, *5*, A135.
(8) Delacourt, C.; Poizot, P.; Morcrette, M.; Tarascon, J.-M.; Masquelier, C. *Chem. Mater.* **2004**, *16*, 93.
(9) Deniard, P.; Dulac, A. M.; Rocquefelte, X.; Grigorova, V.; Lebacq, O.; Pasturel, A.; Jobic, S. *J. Phys. Chem. Solids* **2004**, *65*, 229.
(10) Morgan, D.; Van der Ven, A.; Ceder, G. *Electrochem. Solid-State Lett.* **2004**, *7*, A30.
(11) Tang, P.; Holzwarth, N. A. W. *Phys. Rev. B* **2003**, *68*, 165107.

10.1021/ic048431w CCC: $30.25
Published on Web 02/26/2005

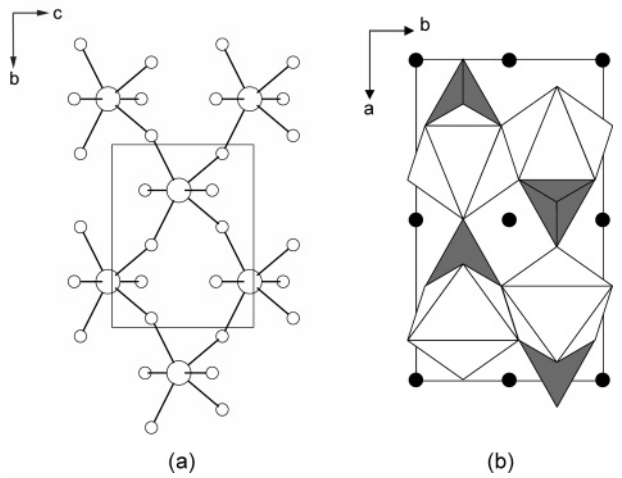

Figure 1. Crystal structure of $LiMPO_4$. (a) A perspective view of the MO_4 layer made up of corner-sharing MO_6 octahedra. (b) A projection view of how the MO_4 layers stack along the *a*-axis direction. In panel b, the PO_4 units are indicated by shaded tetrahedra, the MO_6 octahedra by unshaded octahedra, and the Li atoms by filled circles.

During the past four decades, studies on $LiMPO_4$ (M = Mn, Fe, Co, Ni) have been mostly concerned with their magnetic properties.[12−30] In understanding these properties, it is crucial to know what spin exchange paths between the M^{2+} ions are important. The crystal structure of $LiMPO_4$ is made up of distorted MO_6 octahedra, which share their corners to form MO_4 layers parallel to the *bc*-plane (Figure 1a). These layers are stacked along the *a*-direction such that the P atoms occupy the tetrahedral sites between adjacent layers to form PO_4 units, while the Li atoms occupy the octahedral sites (Figure 1b). Within each MO_4 layer, each M^{2+} ion makes M−O−M superexchange (SE) interactions (J_1) as well as M−O···O−M super-superexchange (SSE) interactions along the *b*-direction (J_b) and along the *c*-direction (J_c) (Figure 2a). Only SSE interactions occur between adjacent MO_4 layers. The interlayer SSE path for J_2 occurs along the *b*-direction, and the interlayer SSE paths for J_3 and J_4 along the *c*-direction (Figure 2a,b).

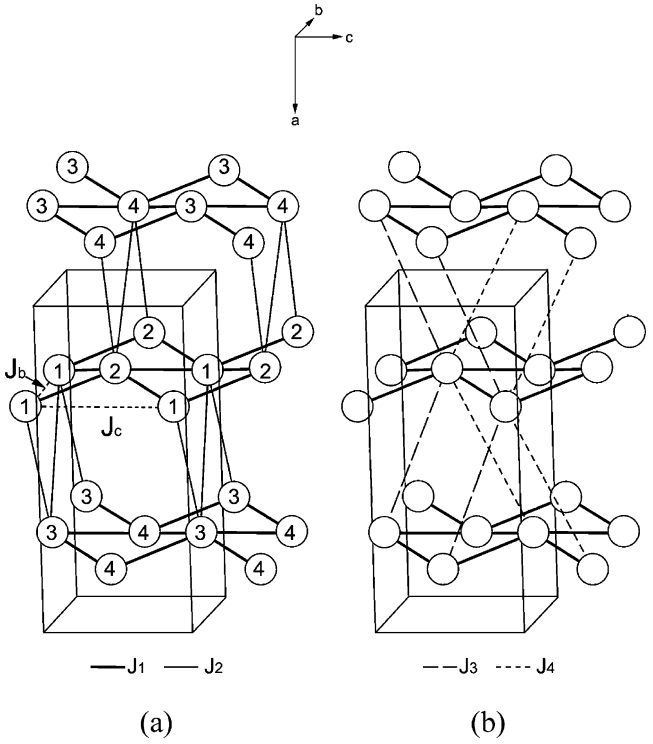

Figure 2. Schematic view of the arrangement of the transition metal atoms M(*i*) ($i = 1-4$) in $LiMPO_4$ and the spin exchange paths associated with the interactions: (a) J_1, J_b, J_c, and J_2; (b) J_3 and J_4.

Recent studies on a number of magnetic oxides have shown[31−34] that the strength of an M−O···O−M spin exchange is primarily governed by the O···O distance and the ∠M−O···O angles rather than by the M···M distance. In particular, an M−O···O−M spin exchange becomes negligible when its O···O contact is longer than the van der Waals distance (i.e., 2.8 Å). In $LiMPO_4$ (M = Mn, Fe, Co, Ni), the M···M distances in the intra- and interlayer SSE interactions increase in the order $J_c < J_2 < J_3 < J_4 < J_b$ (Table 1). The O···O distances are shorter than 2.8 Å in the SSE paths for J_2, J_3, J_4, and J_b but longer than 2.8 Å in the SSE path for J_c. All other possible interlayer SSE paths not shown in Figure 2 have O···O distances longer than 2.8 Å. Consequently, in describing the magnetic properties of $LiMPO_4$ (M = Mn, Fe, Co, Ni), it would be necessary to consider at least the SE path for J_1 as well as the SSE paths for J_2, J_3, J_4, and J_b unless some of them can be neglected on the basis of appropriate electronic structure calculations.

All $LiMPO_4$ (M = Mn, Fe, Co, Ni) compounds undergo a three-dimensional (3D) antiferromagnetic ordering at low temperatures (T_N = 34.9,[12] 52,[17] 21.8,[21] and 19.1 K[26] for M

(12) Mays, J. M. *Phys. Rev.* **1963**, *131*, 38.
(13) Elliston, P. R.; Creer, J. G.; Troup, G. J. *J. Phys. Chem. Solids* **1969**, *30*, 1335.
(14) Tucker, M. C.; Doeff, M. M.; Richardson, T. J.; Fiñones, R.; Reimer, J. A.; Cairns, E. J. *Electrochem. Solid-State Lett.* **2002**, *5*, A95.
(15) Santoro, R. P.; Newnham, R. E. *Acta Crystallogr.* **1967**, *22*, 344.
(16) Creer, J. C.; Troup, G. J. *Phys. Lett. A* **1970**, *32*, 439.
(17) Rousse, G.; Rodriguez-Carvajal, J.; Patoux, S.; Masquelier, C. *Chem. Mater.* **2003**, *15*, 4082.
(18) Santoro, R. P.; Segal, D. J.; Newnham, R. E. *J. Phys. Chem. Solids* **1966**, *27*, 1192.
(19) Goñi, A.; Lezama, L.; Barberis, G. E.; Pizarro, J. L.; Arriortua, M. I.; Rojo, T. *J. Magn. Magn. Mater.* **1996**, *164*, 251.
(20) Kornev, I.; Bichurin, M.; Rivers, J.-P.; Gentil, S.; Schmid, H.; Jansen, A. G. M.; Wyder, P. *Phys. Rev. B* **2000**, *62*, 12247.
(21) Rivera, J.-P. *J. Korean Phys. Soc.* **1998**, *32*, S1855.
(22) Kornev, I.; Rivera, J.-P.; Gentil, S.; Jansen, A. G. M.; Bichurin, M.; Schmid, H.; Wyder, P. *Physica B* **1999**, *271*, 304.
(23) Karchenko, N. F.; Karchenko, Yu. N.; Szymczak, R.; Baran, M.; Schmid, H. *Low. Temp. Phys.* **2001**, *27*, 895.
(24) Karchenko, N. F.; Desnenko, V. A.; Karchenko, Yu. N.; Szymczak, R.; Baran, M. *Low. Temp. Phys.* **2002**, *28*, 646.
(25) Vankin, D.; Zaretsky, J. L.; Miller, L. L.; Rivera, J.-P.; Schmid, H. *Phys. Rev. B* **2002**, *65*, 224414.
(26) Vankin, D.; Zaretsky, J. L.; Ostenson, J. E.; Chakoumakos, B. C.; Goñi, A.; Pagliuso, P. J.; Rojo, T.; Barberis, G. E. *Phys. Rev. B* **1999**, *60*, 1100.
(27) Chupis, I. E. *Low Temp. Phys.* **2000**, *26*, 419.
(28) Karchenko, Yu. N.; Karchenko, N. F.; Baran, M.; Szymczak, R. *Low. Temp. Phys.* **2003**, *29*, 579.
(29) Arčon, D.; Zorko, A.; Cevc, P.; Dominiko, R.; Bele, M.; Jamnik, J.; Jagličić, Z.; Golosovsky, I. *J. Phys. Chem. Solids* **2004**, *65*, 1773.
(30) Arčon, D.; Zorko, A.; Dominiko, R.; Jagličić, Z. *J. Phys.*: *Condens. Matter* **2004**, *16*, 5531.
(31) Whangbo, M.-H.; Koo, H.-J.; Dai, D. *J. Solid State Chem.* **2003**, *176*, 417 and references therein.
(32) Whangbo, M.-H.; Koo, H.-J.; Dai, D.; Jung, D. *Inorg. Chem.* **2003**, *42*, 3898.
(33) Whangbo, M.-H.; Dai, D.; Koo, H.-J. *Dalton Trans.* **2004**, 3019.
(34) Koo, H.-J.; Whangbo, M.-H.; Lee, K.-S. *Inorg. Chem.* **2003**, *42*, 5932.

Table 1. Geometrical Parameters Associated with the M−O−M Superexchange and M−O···O−M Super-superexchange Paths of $LiMPO_4$ (M = Mn, Fe, Co, Ni)

	Mn	Fe	Co	Ni
(a) M−O-M Superexchange Path J_1				
M···M	3.920	3.870	3.821	3.781
∠M−O−M	125.4	127.5	128.3	129.2
(b) M−O···O−M Super-superexchange Path J_2				
M···M	5.498	5.417	5.404	5.373
O···O	2.469	2.478	2.476	2.497
∠M−O···O	139.0	139.0	139.8	129.1
∠O···O−M	131.1	130.2	130.1	141.2
(c) M−O···O−M Super-superexchange Path J_3				
M···M	5.638	5.580	5.535	5.467
O···O	2.558	2.553	2.546	2.561
∠M−O···O	93.7	93.4	156.1	159.4
∠O···O−M	155.4	154.0	94.5	96.4
(d) M−O···O−M Super-superexchange Path J_4				
M···M	5.858	5.776	5.697	5.605
O···O	2.469	2.448	2.476	2.497
∠M−O···O	139.0	139.0	139.8	141.2
∠O···O−M	103.4	102.0	101.5	101.7
(e) M−O···O−M Super-superexchange Path J_b				
M···M	6.100	6.010	5.920	5.854
O···O	2.450	2.447	2.432	2.413
∠M−O···O	149.0	149.7	148.2	147.0
∠O···O−M	149.0	149.7	148.2	147.0
(f) M−O···O−M Super-superexchange Path J_c				
M···M	4.744	4.692	4.700	4.677
M−O	2.130	2.251	2.076	2.049
O···O	3.076	2.976	2.986	2.928
O−M	2.282	2.064	2.200	2.143
∠M−O···O	89.7	91.4	91.1	93.8
∠O···O−M	105.1	107.3	107.8	108.4

= Mn, Fe, Co, and Ni, respectively). In the 3D antiferromagnetic structures of $LiMPO_4$, the M^{2+} ions of the MO_4 layers are antiferromagnetically coupled, and the adjacent MO_4 layers are antiferromagnetically coupled.[15,17,18,25,26] In their neutron diffraction study of $LiFePO_4$,[17] Rousse et al. discussed the phase diagram of its magnetic structure in terms of the three spin exchange interactions J_1, J_2, and J_b (in their analysis, the exchange interactions J_3 and J_4 were not included). Since the values of J_1, J_2, and J_b are unknown, they examined the phase diagram as a function of J_1 and J_2 for the cases of $J_b > 0$ and $J_b < 0$. Weak ferromagnetism is found below T_N for $LiMnPO_4$,[29] $LiCoPO_4$,[23] and $LiNiPO_4$,[28] but not for $LiFePO_4$.[30] The weak ferromagnetism of $LiCoPO_4$ and $LiNiPO_4$ was explained by assuming a spin structure modulation[22] along one crystallographic direction, and that of $LiNiPO_4$ by supposing an "angled cross" type antiferromagnetic configuration.[27] In contrast, spin frustration and magnetic excitations of soliton type were suggested to cause the weak ferromagnetism of $LiMnPO_4$.[30] As mentioned by Rousse et al. for $LiFePO_4$,[17] the spin lattice of $LiMPO_4$ can in principle be subject to geometric spin frustration,[39,40] if the SSE interactions, J_b and J_2, are both strongly antiferromagnetic. To see the possibility of geometric spin frustration in $LiMPO_4$ and understand the observed 3D antiferromagnetic structures of $LiMPO_4$, it is necessary to determine the strengths of their spin exchange interactions J_1, J_2, J_3, J_4, and J_b.

So far, there has been no systematic study aimed at explaining the magnetic structures of $LiMPO_4$ (M = Mn, Fe, Co, Ni) in terms of their spin exchange parameters determined from electronic structure calculations. In the present work we evaluate the relative strengths of their spin exchange parameters J_1, J_b, J_2, J_3, and J_4 on the basis of spin dimer analysis using the extended Hückel tight binding calculations and also electronic band structure analysis using first principles density functional theory (DFT) calculations.[31] We then discuss the ordered magnetic structures of $LiMPO_4$ (M = Mn, Fe, Co, Ni) expected from these spin exchange parameters using the classical spin approximation.

2. Structural Parameters of Spin Exchange Paths

$LiMPO_4$ has two equivalent MO_4 layers and four equivalent M atoms per unit cell (Table 2). The M^{2+} ions of each MO_4 layer have a corrugated arrangement, and every M^{2+} ion makes four equivalent SE interactions J_1 in each MO_4 layer and two SSE interactions J_b along the *b*-direction (Figure 2a). The corrugated MO_4 layers are stacked along the *a*-axis direction such that the SSE paths for J_2 with the shortest interlayer M···M distance occur along the *b*-direction (Figure 2a). Two different interlayer SSE interactions with the O···O distance shorter than 2.8 Å (i.e., J_3 and J_4) occur along the *c*-direction (Figure 2b). The geometrical parameters associated with the SE path for J_1 and the SSE paths for J_2, J_3, J_4, J_b, and J_c are summarized in Table 1.

3. Spin Dimer Analysis

The spin exchange parameter J is written as $J = J_F + J_{AF}$, where the ferromagnetic term J_F is positive and the antiferromagnetic term J_{AF} is negative. In general, J_F is very small so that the trends in the J values are well approximated by those in the corresponding J_{AF} values. When there are N unpaired spins per spin site, the J_{AF} term is approximated by[31]

$$J_{AF} \approx -\frac{\langle(\Delta e)^2\rangle}{U_{eff}} \tag{1}$$

where the effective on-site repulsion U_{eff} is essentially a constant for a given system. The $\langle(\Delta e)^2\rangle$ term is further approximated by[31]

$$\langle(\Delta e)^2\rangle \approx \frac{1}{N^2}\sum_{\mu=1}^{N}(\Delta e_{\mu\mu})^2 \tag{2}$$

where $\Delta e_{\mu\mu}$ is the energy split that results when two magnetic orbitals ϕ_μ on adjacent spin sites interact.

The high-spin M^{2+} cations of $LiMPO_4$ are located in a distorted octahedral environment, so that the cation electron configuration can be written as $(t_{2g})^3(e_g)^2$ for Mn^{2+}, $(t_{2g})^4(e_g)^2$ for Fe^{2+}, $(t_{2g})^5(e_g)^2$ for Co^{2+}, and $(t_{2g})^6(e_g)^2$ for Ni^{2+}. Thus, $N = 5$ for Mn^{2+}, $N = 4$ for Fe^{2+}, $N = 3$ for Co^{2+}, and

(35) Geller, S.; Durand, J.-L. *Acta Crystallogr.* **1960**, *13*, 325.
(36) Streltsov, V. A.; Belokoneva, E. L.; Tsirelson, V. G.; Hansen, N. K. *Acta Crystallogr., Sect. B* **1993**, *49*, 147.
(37) Kubel, F. *Z. Kristallogr.* **1994**, *209*, 755.
(38) Abrahams, I.; Easson, K. S. *Acta Crystallogr., Sect C* **1993**, *49*, 925.
(39) Greedan, J. E. *J. Mater. Chem.* **2001**, *11*, 37 and references therein.
(40) Dai, D.; Whangbo, M.-H. *J. Chem. Phys.* **2004**, *121*, 672.

Table 2. Positions of the Four Metal Atoms M(i) ($i = 1-4$) in the Unit Cell of $LiMPO_4$ in Fractional Coordinates[a]

spin site	x	y	z
M(1)	x_0	$^1/_4$	z_0
M(2)	$^1/_2 - x_0$	$^3/_4$	$^1/_2 + z_0$
M(3)	$-x_0$	$^3/_4$	$-z_0$
M(4)	$^1/_2 + x_0$	$^1/_4$	$^1/_2 - z_0$

[a] $x_0 = 0.2817$ and $z_0 = 0.9719$ for Mn (ref 35), $x_0 = 0.2822$ and $z_0 = 0.9747$ for Fe (ref 36), $x_0 = 0.2786$ and $z_0 = 0.9793$ for Co (ref 37), and $x_0 = 0.2756$ and $z_0 = 0.9825$ for Ni (ref 38).

$N = 2$ for Ni^{2+}. If we represent the numbers of unpaired spins in the t_{2g}- and e_g-block levels by n_t and n_e, respectively, $n_t = 3$ and $n_e = 2$ for Mn^{2+}, $n_t = 2$ and $n_e = 2$ for Fe^{2+}, $n_t = 1$ and $n_e = 2$ for Co^{2+}, and $n_t = 0$ and $n_e = 2$ for Ni^{2+}. For simplicity, the t_{2g}-block levels of each spin site may be labeled as ϕ_1, ϕ_2, and ϕ_3, and the e_g-block levels of each spin site as ϕ_4 and ϕ_5. By defining the energy terms

$$(\Delta e_{t_{2g}})^2 = (\Delta e_{11})^2 + (\Delta e_{22})^2 + (\Delta e_{33})^2$$
$$(\Delta e_{e_g})^2 = (\Delta e_{44})^2 + (\Delta e_{55})^2 \quad (3)$$

the $\langle(\Delta e)^2\rangle$ term is approximated by[31,41]

$$\langle(\Delta e)^2\rangle \approx \frac{1}{N^2}\left[\frac{n_t^2}{9}(\Delta e_{t_{2g}})^2 + \frac{n_e^2}{4}(\Delta e_{e_g})^2\right] \quad (4)$$

For a variety of magnetic solids, it has been found[31] that their magnetic properties are well described by the $\langle(\Delta e)^2\rangle$ values obtained from extended Hückel tight binding calculations, when both the d orbitals of M and the s/p orbitals of its surrounding ligands are represented by double-ζ Slater type orbitals.[42] The $\langle(\Delta e)^2\rangle$ values for the exchange interactions J_1, J_b, J_2, J_3, and J_4 of $LiMPO_4$ (M = Mn, Fe, Co, Ni) were calculated by employing the atomic orbital parameters of Table 3.[43]

The $\langle(\Delta e)^2\rangle$ values summarized in Table 4 reveal that the intralayer SE interaction J_1 is more strongly antiferromagnetic than are the SSE interactions J_2, J_3, J_4, and J_b. The intralayer SSE interaction J_b is comparable in strength to the interlayer SSE interaction J_2. The SSE interactions J_3 and J_4 are negligibly weaker than the J_2 and J_b interactions. Since the M···M distances of the SSE paths increase in the order $J_2 < J_3 < J_4 < J_b$, the short M···M distance does not necessarily guarantee that the associated M−O···O−M spin exchange is strong. Table 1 shows that both ∠M−O···O angles of the M−O···O−M spin exchange path are large in the strong spin exchange interactions J_b and J_2, but this is not the case for the weak spin exchange interactions J_3 and J_4. These observations reinforce the conclusion[31−34] from the studies of other magnetic oxides that the strength of an M−O···O−M spin exchange is mainly governed by the O···O distance and the ∠M−O···O angles rather than by the M···M distance.

Table 3. Exponents ζ_i and Valence Shell Ionization Potentials H_{ii} of Slater Type Orbitals χ_i Used for Extended Hückel Tight Binding Calculation[a]

atom	χ_i	H_{ii} (eV)	ζ_i	C_1[b]	ζ_i'	C_2[b]
Mn	4s	−9.75	1.844	1.0		
Mn	4p	−5.89	1.350	1.0		
Mn	3d	−11.67	5.767	0.3898	2.510	0.7297
Fe	4s	−9.10	1.925	1.0		
Fe	4p	−5.32	1.390	1.0		
Fe	3d	−12.6	6.068	0.4038	2.618	0.7198
Co	4s	−9.21	2.001	1.0		
Co	4p	−5.29	1.430	1.0		
Co	3d	−13.18	6.386	0.4133	2.745	0.7126
Ni	4s	−9.17	2.077	1.0		
Ni	4p	−5.15	1.470	1.0		
Ni	3d	−13.49	6.706	0.4212	2.874	0.7066
O	2s	−32.3	2.688	0.7076	1.675	0.3745
O	2p	−14.8	3.694	0.3322	1.659	0.7448

[a] H_{ii}'s are the diagonal matrix elements $\langle\chi_i|H^{eff}|\chi_i\rangle$, where H^{eff} is the effective Hamiltonian. In our calculations of the off-diagonal matrix elements $H^{eff} = \langle\chi_i|H^{eff}|\chi_j\rangle$, the weighted formula was used. See: Ammeter, J.; Bürgi, H.-B.; Thibeault, J.; Hoffmann, R. *J. Am. Chem. Soc*. **1978**, *100*, 3686. [b] Coefficients used in the double-ζ Slater type orbital expansion.

Table 4. $\langle(\Delta e)^2\rangle$ Values in $(meV)^2$ Calculated for the Spin Exchange Paths for J_1, J_b, J_2, J_3, and J_4 of $LiMPO_4$ (M = Mn, Fe, Co, Ni)

	J_1	J_b	J_2	J_3	J_4
Mn	890	70	54	15	7
Fe	830	364	250	37	29
Co	2600	1174	837	4	5
Ni	8600	3978	2600	0	0

Table 4 shows that the magnetic structures of $LiMPO_4$ (M = Mn, Fe, Co, Ni) can be well described using only the three spin exchange parameters J_1, J_2, and J_b. In terms of these parameters, we now consider the magnetic ground state expected for $LiMPO_4$ (M = Mn, Fe, Co, Ni). Since J_1 is stronger than J_b, each MO_4 layer should form an antiferromagnetic plane, as depicted in Figure 3. These antiferromagnetic planes should be antiferromagnetically coupled by the SSE interactions J_2, hence forming a 3D antiferromagnetic lattice. This prediction is in good agreement with experiment.[15,17,18,25,26] Finally, it is noted that geometric spin frustration associated with the spin exchanges J_b and J_2 is unimportant because J_1 is more strongly antiferromagnetic than J_b and J_2.

4. Electronic Band Structure Analysis

Our discussion in the previous section shows that the spin exchange interactions J_1, J_b, and J_2 are important, and the remaining spin exchange interactions can be neglected. In this section we determine quantitatively the J_1, J_b, and J_2 values of $LiMPO_4$ on the basis of spin-polarized electronic band structure calculations within the framework of first principles density functional theory. The values of J_1, J_b, and J_2 can be determined by mapping the energy differences of the Ising spin Hamiltonian onto those of the electronic Hamiltonian for $LiMPO_4$.[31] Since there are three parameters to determine, it is necessary to consider four different ordered spin states of $LiMPO_4$. In the present work, we employ the four ordered spin arrangements depicted in Figure 4, i.e.,

(41) Whangbo, M.-H.; Koo, H.-J.; Dumas, J.; Continentino, M. A. *Inorg. Chem*. **2002**, *41*, 2193.
(42) Clementi, E.; Roetti, C. *Atomic Data Nuclear Data Tables* **1974**, *14*, 177.
(43) Our calculations were carried out by employing the SAMOA (Structure and Molecular Orbital Analyzer) program package (Dai, D.; Ren, J.; Liang, W.; Whangbo, M.-H. http://chvamw.chem.ncsu.edu/, 2002).

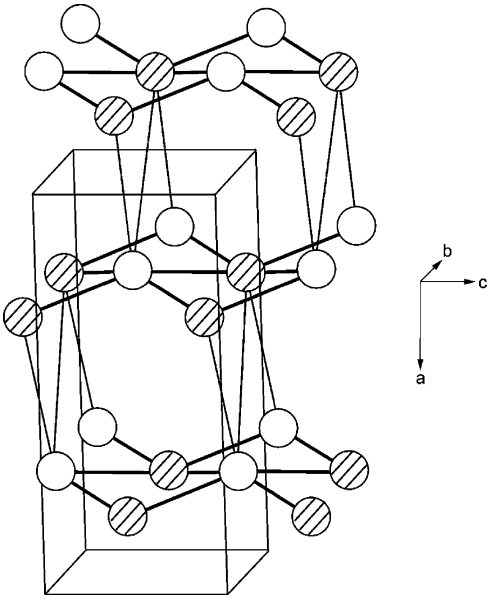

Figure 3. Schematic representations of the magnetic ground state expected for $LiMPO_4$. Up spins and down spins are represented by empty and filled circles, respectively. The spin exchange paths for J_1 are represented by thick solid lines, and the spin exchange paths for J_2 by thin solid lines.

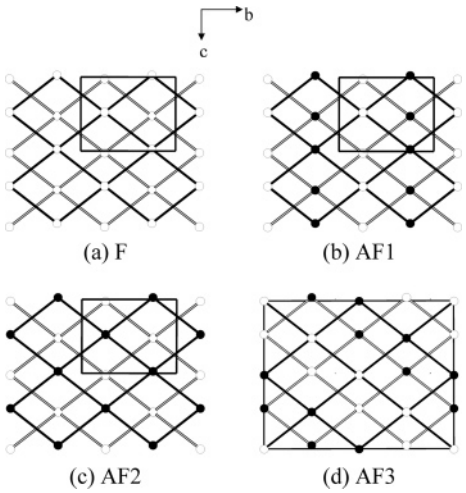

Figure 4. Schematic representations of the four ordered spin arrangements employed for the evaluation of the spin exchange parameters J_1, J_b, and J_2 on the basis of electronic band structure calculations: (a) F, (b) AF1, (c) AF2, and (d) AF3 states. The rectangular boxes represent the unit cells.

the spin arrangements F, AF1, AF2, and AF3. These states are magnetic insulating states, so that we describe their electronic structures by spin-polarized electronic band structure calculations.

Our calculations for the four ordered spin states F, AF1, AF2, and AF3 of $LiMPO_4$ (M = Mn, Fe) were carried out using the full-potential linearized augmented plane wave method embodied in the WIEN2k code[44] and the Perdew−Burke−Ernzerhof generalized gradient approximation[45] for the exchange and correlation correction. The maximum l value in the expansion of the basis set inside each atomic sphere was 12 for the computation of muffin-tin matrix elements and 4 for that of the non-muffin-tin matrix elements. The convergence of the basis set was controlled by a cutoff parameter $R_{mt}K_{max} = 7$, where R_{mt} is the smallest atomic sphere radius in the unit cell and K_{max} is the magnitude of the largest **k** vector. The self-consistency was carried out on a 200 **k**-points mesh in the full Brillouin zone, with atomic sphere radii of 2 au for Li, Fe, and Mn, 1.45 au for P, 1.4 au for O and $G_{MAX} = 14$ bohr^{-1}.

For the analysis of the spin exchange interactions in $LiMPO_4$ (M = Co, Ni), the above approach fails because it predicts that the F state is more stable than the AF1 state in disagreement with experiment. To properly describe the spin exchange interactions of these phosphates, it is necessary to go beyond the level of calculations employed in the present work. Our LDA+U electronic band structure analysis of $LiMPO_4$ (M = Co, Ni) will be reported at a later time.

The high-spin M^{2+} ion of $LiMPO_4$ has more than one unpaired spin. Therefore, in describing the 3D spin lattice of $LiMPO_4$ in terms of the Ising spin Hamiltonian,[31,46,47] one needs to take into consideration how this affects the energy-difference mapping analysis. The Ising Hamiltonian of a spin dimer is written as

$$\hat{H} = -J\hat{S}_{1z}\hat{S}_{2z} \tag{5}$$

where J is the spin exchange parameter, and $\hat{S}_{1z}$ and $\hat{S}_{2z}$ are the z-components of the spin angular momentum operators at the spin sites 1 and 2, respectively. Suppose that each spin site has N unpaired spins. Then, under the Ising Hamiltonian of eq 1, the energies of the highest spin (HS) and broken symmetry (BS) states are given by[46,47]

$$E_{HS} = -\frac{N^2}{4}J \quad \text{and} \quad E_{BS} = +\frac{N^2}{4}J \tag{6}$$

so that the energy difference $\Delta E = E_{BS} - E_{HS}$ is expressed as

$$\Delta E = \frac{N^2}{2}J \tag{7}$$

Consequently, the J parameter is obtained from eq 7 by calculating the ΔE value in terms of electronic structure calculations. In a similar manner, when the spin lattice of $LiMPO_4$ is described by the Ising Hamiltonian consisting of the three spin exchange parameters J_1, J_b, and J_2, the total spin exchange energies (per formula unit) of the F, AF1, AF2, and AF3 states are written as

$$E_F = (N^2/4)(-2J_1 - J_2 - J_b) \tag{8a}$$

$$E_{AF1} = (N^2/4)(2J_1 + J_2 - J_b) \tag{8b}$$

$$E_{AF2} = (N^2/4)(-2J_1 + J_2 - J_b) \tag{8c}$$

$$E_{AF3} = (N^2/4)J_b \tag{8d}$$

(44) Blaha, P.; Schwarz, K.; Madsen, G.; Kvasnicka, D.; Luitz, J., *WIEN2k*, An Augmented Plane Wave + Local Orbitals Program for Calculating Crystal Properties (Karlheinz Schwarz, Techn. Universität Wien, Austria), 2001. ISBN 3-9501031-1-2. See also http://www.wien2k.at/.

(45) Perdew, J. P.; Burke, S.; Ernzerhof, M. *Phys. Rev. Lett.* **1996**, *77*, 3865.

(46) Dai, D.; Whangbo, M.-H. *J. Chem. Phys.* **2001**, *114*, 2887.

(47) Dai, D.; Whangbo, M.-H. *J. Chem. Phys.* **2003**, *118*, 29.

Table 5. Spin Exchange Parameters in meV Calculated for the Spin Exchange Paths for J_1, J_b, and J_2 of $LiMPO_4$ (M = Mn, Fe)

	J_1	J_b	J_2
Mn	−1.16	0.38	−0.50
Fe	−1.08	−0.40	−0.92

From eqs 8a−c, the spin exchange parameters J_1 and J_2 are related to the state energy differences as

$$J_1 = (4/N^2)(E_{AF1} - E_{AF2})/4 \quad (9a)$$

$$J_2 = (4/N^2)(E_{AF2} - E_F)/2 \quad (9b)$$

Therefore, the J_1 and J_2 values are readily estimated once the energies of the F, AF1, and AF2 states are calculated on the basis of spin-polarized electronic band structure calculations. Using these J_1 and J_2 values, J_b can be determined by combining eq 8d with any one of eqs 8a−c. Table 5 summarizes the J_1, J_b, and J_2 values thus calculated for $LiMPO_4$ (M = Mn, Fe).

Table 5 shows that J_1 is more strongly antiferromagnetic than J_b and J_2, in agreement with the conclusion from the $\langle(\Delta e)^2\rangle$ values estimated in the previous section. The electronic band structure analysis differs from the spin dimer analysis mainly on the nature of the intralayer spin exchange J_b. For $LiFePO_4$, J_b is antiferromagnetic in the electronic band structure analysis as in the case of the spin dimer analysis. In contrast to the case of the spin dimer analysis, however, J_b is more weakly antiferromagnetic than J_2 in the electronic band structure analysis. For $LiMnPO_4$, J_b is ferromagnetic in the electronic band structure analysis in contrast to the case of the spin dimer analysis.

Nevertheless, the electronic band structure analysis predicts the same magnetic structure for $LiMPO_4$ (M = Mn, Fe) as does the spin dimer analysis, because both analyses predict that J_1 and J_2 are antiferromagnetic, and J_1 is more strongly antiferromagnetic than is J_b. For both $LiMnPO_4$ and $LiFePO_4$, the J_2/J_1 ratio is substantial (i.e., 0.44 and 0.84, respectively) so that their magnetic structures should be described as strongly coupled antiferromagnetic planes rather than as weakly coupled antiferromagnetic planes. Furthermore, the J_b and J_2 interactions cannot induce geometric spin frustration in $LiMnPO_4$ because J_b is ferromagnetic while J_2 is antiferromagnetic. The J_b and J_2 interactions are not expected to cause geometric spin frustration in $LiFePO_4$ either, because J_b is more weakly antiferromagnetic than J_2. Consequently, for the magnetic structure and the geometric spin frustration of $LiMPO_4$ (M = Mn, Fe), the same conclusions are reached by the spin dimer and electronic band structure analyses.

To examine how quantitatively accurate the calculated J_1, J_b, and J_2 parameters are, we discuss the Curie−Weiss temperatures θ of $LiMPO_4$ (M = Mn, Fe) under the mean field approximation, in which θ is related to the spin exchange parameters as[48]

$$\theta = \frac{S(S+1)}{3k_B}\sum_i z_i J_i \quad (10)$$

The summation is over sets of the equivalent magnetic sites i from a chosen magnetic site, and z_i is the number of equivalent magnetic neighbors with the spin exchange parameter J_i. According to Figure 2a, the summation around each spin site includes $4J_1$, $2J_b$, and $2J_2$. In addition, S = 5/2 and 2 for the high-spin Mn^{2+} and Fe^{2+} ions, respectively. Thus, according to eq 10, the J_1, J_b, and J_2 values of Table 5 lead to the θ values of −164 K for $LiMnPO_4$ and −162 K for $LiFePO_4$. The corresponding experimental θ values deduced from the magnetic susceptibility data are −87 K for $LiMnPO_4$[29] and −115 K for $LiFePO_4$.[30] Thus, the calculated J_1, J_b, and J_2 values are overestimated by a factor of 2. DFT calculations tend to overestimate the magnitude of spin exchange interactions by a factor of up to 4.[46,49,50]

5. Classical Spin Analysis of Ordered Magnetic Structures

In this section, we examine the relative stabilities of various ordered spin arrangements of $LiMPO_4$ to confirm that the magnetic structure shown in Figure 3 is indeed the magnetic ground state. For this purpose we employ the method of Freiser,[51] which assumes that spins can adopt all possible directions in space (the classical spin approximation), the orientational distributions of the spins are independent, and the spin exchange interactions are isotropic. This method has recently been employed to examine the ordered spin arrangements of several magnetic solids.[33,52] Consider an ordered spin arrangement in which the spin sites μ (=1, 2, ..., m) of the unit cell located at the coordinate origin (i.e., the lattice vector $\mathbf{R} = 0$) have the mean spins $\boldsymbol{\sigma}_\mu^0$. Then, for a magnetic solid with repeat vectors **a**, **b**, and **c**, the ordered spin arrangement can be described in terms of the "Bloch" spin functions $\sigma_\mu(\mathbf{k})$,

$$\boldsymbol{\sigma}_\mu(\mathbf{k}) = \frac{1}{\sqrt{N}}\sum_{\mathbf{R}} \boldsymbol{\sigma}_\mu^0 \exp(i\mathbf{k}\cdot\mathbf{R}) \quad (11)$$

where N is the number of unit cells in the magnetic solid, and **R** and **k** are the lattice and wave vectors, respectively. Then, the spin exchange interaction energy $\xi_{\mu\nu}(\mathbf{k})$ between two Bloch spin functions $\boldsymbol{\sigma}_\mu(\mathbf{k})$ and $\boldsymbol{\sigma}_\nu(\mathbf{k})$ is given by

$$\xi_{\mu\nu}(\mathbf{k}) = -\sum_{\mathbf{R}} J_{\mu\nu}(\mathbf{R}) \exp(i\mathbf{k}\cdot\mathbf{R}) \quad (12)$$

and the diagonalization of the interaction matrix $\boldsymbol{\Xi}(\mathbf{k})$,

$$\boldsymbol{\Xi}(\mathbf{k}) = \begin{pmatrix} \xi_{11}(\mathbf{k}) & \xi_{12}(\mathbf{k}) & ... & \xi_{1m}(\mathbf{k}) \\ \xi_{21}(\mathbf{k}) & \xi_{22}(\mathbf{k}) & ... & \xi_{2m}(\mathbf{k}) \\ ... & ... & ... & ... \\ \xi_{m1}(\mathbf{k}) & \xi_{m2}(\mathbf{k}) & ... & \xi_{mm}(\mathbf{k}) \end{pmatrix} \quad (13)$$

leads to the eigenvalues $E_i(\mathbf{k})$ ($i = 1 - m$). The associated

(48) Kahn, O. *Molecular Magnetism*; VCH: Weinheim, 1993.
(49) Dai, D.; Koo, H.-J.; Whangbo, M.-H. *J. Solid State Chem.* **2003**, *175*, 341.
(50) Grau-Crespo, R.; de Leeuw, N. H.; Catlow, C. R. *J. Mater. Chem.* **2003**, *13*, 2848.
(51) Freiser, M. J. *Phys. Rev.* **1961**, *123*, 2003.
(52) Dai, D.; Koo, H.-J.; Whangbo, M.-H. *Inorg. Chem.* **2004**, *43*, 4026.

eigenfunctions $\psi_i(\mathbf{k})$ ($i = 1 - m$) are described by the linear combination of the Bloch spin functions $\boldsymbol{\sigma}_\mu(\mathbf{k})$,

$$\psi_i(\mathbf{k}) = \sum_{\mu=1}^{m} C_{\mu i}(\mathbf{k})\boldsymbol{\sigma}_\mu(\mathbf{k}) \tag{14}$$

The presence of up or down spin at a spin site μ is described by the sign of the coefficient $C_{\mu i}(\mathbf{k})$. For a given set of spin exchange parameters, one can determine the value of $\mathbf{k}$ that leads to the minimum energy, $E_{\min}$, of $E_i(\mathbf{k})$, which occurs from the lowest-lying band $E_1(\mathbf{k})$. This particular $\mathbf{k}$ point, denoted by $\boldsymbol{k}_{\min}$, has a specific meaning. For example, $\mathbf{k}_{\min} = (0, 0, 0)$ means that the magnetic unit cell is the same as the chemical unit cell, while $\mathbf{k}_{\min} = (1/2, 0, 0)$ means that the magnetic ordering doubles the unit cell length along the *a*-direction.

The nonzero contributions to the matrix elements $\xi_{\mu\nu}(\mathbf{k})$ from the spin exchange paths J_1, J_b, and J_2 between the spin sites μ and ν (μ, $\nu = 1-4$) of $LiMPO_4$ are summarized in Table 6. As representative examples, the $E_i(\mathbf{k})$ vs $\mathbf{k}$ plots calculated for $LiMnPO_4$ and $LiFePO_4$ (using the relative J_1, J_2, and J_b values deduced from the electronic band structure analysis) are presented in Figure 5a,b, respectively. In both cases, $\mathbf{k}_{\min} = \Gamma = (0, 0, 0)$, so that the magnetic unit cell is the same as the chemical unit cell, namely, the magnetic ordering does not increase the unit cell size. This is in agreement with experiment. The spin arrangements described by $\psi_1(\mathbf{k}_{\min})$ are identical with the magnetic structure shown in Figure 3. Though not shown, we reach the same conclusion for $LiMnPO_4$ (M = Mn, Fe, Co, Ni) when the $E_i(\mathbf{k})$ vs $\mathbf{k}$ plots are calculated by using the relative J_1, J_2, and J_b values deduced from the spin dimer analysis.

Table 6. Nonzero Contributions to the Matrix Elements $\xi_{\mu\nu}(\mathbf{k})$ from the Spin Exchange Paths between the Spin Sites μ and ν (μ, $\nu = 1-4$) of $LiMPO_4$[a,b]

μ	ν	cell	M···M	contribution to $\xi_{\mu\nu}(\mathbf{k})$
1	1	[0, −1, 0]	d_b	$-J_b \exp(-i2\pi x_b)$
1	2	[0, −1, 0]	d_1	$-J_1 \exp(-i2\pi x_b)$
		[0, −1, 1]	d_1	$-J_1 \exp[i2\pi(-x_b + x_c)]$
		[0, 0, 0]	d_1	$-J_1$
		[0, 0, 1]	d_1	$-J_1 \exp(i2\pi x_c)$
1	3	[0, −1, 1]	d_2	$-J_2 \exp[i2\pi(-x_b + x_c)]$
		[0, 0, 1]	d_2	$-J_2 \exp(i2\pi x_c)$
2	4	[−1, 0, 0]	d_2	$-J_2 \exp(-2\pi x_a)$
		[−1, 1, 0]	d_2	$-J_2 \exp[i2\pi(-x_a + x_b)]$

[a] $\xi_{11}(\mathbf{k}) = \xi_{22}(\mathbf{k}) = \xi_{33}(\mathbf{k})$, $\xi_{34}(\mathbf{k}) = \xi_{12}^*(\mathbf{k})$. [b] $d_b = 6.100$ for Mn, 6.010 for Fe, 5.920 for Co, and 5.854 for Ni; $d_1 = 3.920$ for Mn, 3.870 for Fe, 3.821 for Co, and 3.781 for Ni; $d_2 = 5.498$ for Mn, 5.417 for Fe, 5.404 for Co, and 5.373 for Ni.

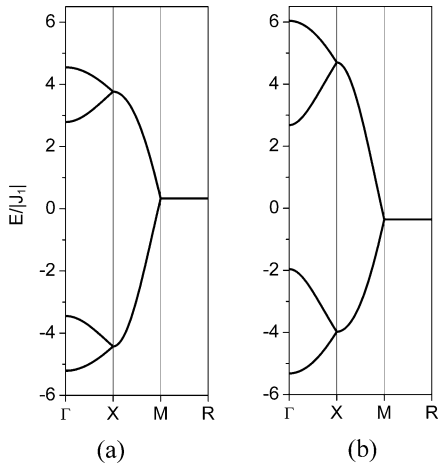

Figure 5. $E_i(\mathbf{k})$ vs $\mathbf{k}$ calculated for $LiMnPO_4$ and $LiFePO_4$ using the classical spin approximation. (a) $LiMnPO_4$ using $J_1 = -1.00$, $J_2 = -0.44$, and $J_b = +0.33$. (b) $LiFePO_4$ using $J_1 = -1.00$, $J_2 = -0.84$, and $J_b = -0.36$. In terms of the reduced reciprocal vectors, the special $\mathbf{k}$-points are defined as follows: $\Gamma = (0, 0, 0)$, X = (0.5, 0, 0), M = (0.5, 0.5, 0), and R = (0.5, 0.5, 0.5).

6. Concluding Remarks

On the basis of the crystal structure of $LiMPO_4$ (M = Mn, Fe, Co, Ni) alone, the SE path J_1 as well as the SSE paths J_2, J_3, J_4, and J_b would be needed in describing the magnetic properties of $LiMPO_4$. Of these five spin exchange paths, only the three paths J_1, J_2, and J_b are essential according to the spin dimer analysis. In agreement with experiment, these three parameters predict that the SE interactions J_1 of each MO_4 layer form an antiferromagnetic plane, and these MO_4 layers are antiferromagnetically coupled by the SSE interactions J_2. The electronic band structure analysis for $LiMnPO_4$ and $LiFePO_4$ shows that J_1 is more strongly antiferromagnetic than J_b and J_2 in agreement with the spin dimer analysis, that their magnetic structures should be described as strongly coupled antiferromagnetic planes, and that the spin exchanges J_b and J_2 do not induce spin frustration in $LiMnPO_4$, nor in $LiFePO_4$. The classical spin analysis in terms of the three parameters J_1, J_2, and J_b shows that the magnetic ordering of $LiMPO_4$ does not increase the unit cell size and the ordered magnetic structure (Figure 3) predicted by J_1, J_2, and J_b is indeed the magnetic ground state.

Acknowledgment. The work at NCSU was supported by the Office of Basic Energy Sciences, Division of Materials Sciences, U.S. Department of Energy, under Grant DE-FG02-86ER45259. The authors thank CCIPL for generous computing resources.

IC048431W